

## Influence of the primary components of the high-speed train on fire heat release rate

YUANLONG ZHOU<sup>a\*</sup>  
HAIQUAN BI<sup>b</sup>  
HONGLIN WANG<sup>b</sup>

<sup>a</sup> University of Science and Technology of China, State Key Laboratory of Fire Science, Hefei, Anhui 230026, China

<sup>b</sup> Southwest Jiaotong University, School of Mechanical Engineering, Chengdu 610031, China

**Abstract** A numerical model of the high-speed train carriage fire is established in this study. The influence of ceilings, sidewalls, luggage racks, seats, and floors on the heat release rate (HRR) of the high-speed train is studied by numerical methods. The results indicate that the heat release rate per unit area (HRRPUA) of ceiling and seat material dramatically influences the peak HRR and the time to peak HRR of train carriage fire. When the peak HRRPUA of interior ceiling material 1 decreases from 326 to 110 kW/m<sup>2</sup>, the peak HRR of the high-speed train fire decreases from 36.4 to 16.5 MW, with a reduction ratio of 54.7%. When seat materials with low HRRPUA are used, the peak HRR reduction ratio is 44.8%. The HRRPUA of the sidewall, luggage rack, and floor materials has little effect on the peak HRR of the carriage fire. However, the non-combustible luggage rack can delay the time when the HRR reaches its peak.

**Keywords:** High-speed train; Carriage fire; Primary components; Heat release rate; Numerical methods

### Nomenclature

$C_s$  – Smagorinsky constant  
 $D_i$  – component mass diffusion coefficient, m<sup>2</sup>/s  
 $f$  – force (except gravity), N

---

\*Corresponding Author. Email: [zylong505@163.com](mailto:zylong505@163.com)

|                |   |   |
|----------------|---|---|
| $g$            | – | gravitational acceleration, $\text{m/s}^2$  |
| $h_s$          | – | sensible enthalpy, $\text{J/kg}$  |
| $k$            | – | coefficient of heat conductivity, $\text{W}/(\text{m K})$                                     |
| $\dot{m}_i'''$ | – | mass formation rate of the $i$ th component in unit volume, $\text{kg}/(\text{m}^3 \text{s})$ |
| $Q$            | – | heat release rate of the fire, $\text{kW}$  |
| $\mathbf{q}_r$ | – | radiant heat flux vector  |
| $P$            | – | pressure, $\text{Pa}$   |
| $R_g$          | – | specific gas constant, $\text{J}/(\text{kg K})$   |
| $S_{ij}$       | – | strain tensor   |
| $T$            | – | thermodynamic temperature, $\text{K}$   |
| $t$            | – | time, $\text{s}$  |
| $U$            | – | velocity of airflow, $\text{m/s}$   |
| $u$            | – | velocity vector   |
| $u_i, u_j$     | – | velocity components, $\text{m/s}$   |
| $x$            | – | distance along the train carriage centre line   |
| $x_i, x_j$     | – | Cartesian coordinates   |
| $Y_i$          | – | volume fraction of the $i$ th component   |

#### Greek symbols

|                    |   |  |
|--------------------|---|--|
| $\mu$              | – | kinematic viscosity, $\text{m}^2/\text{s}$ |
| $\mu_{\text{LES}}$ | – | turbulent viscosity coefficient            |
| $\rho$             | – | density, $\text{kg}/\text{m}^3$            |
| $\tau_{ij}$        | – | residual stress tensor                     |

#### Acronyms

|        |   |                                 |
|--------|---|---------------------------------|
| HRR    | – | heat release rate               |
| HRRPUA | – | heat release rate per unit area |
| LES    | – | large eddy simulation           |

## 1 Introduction

The high-speed train has been favoured by the rail transportation industry worldwide. In the past decade, China's high-speed railway has developed rapidly. By the end of 2022, the mileage of the high-speed railway in China has exceeded 42 000 km. High-speed railways and trains have become an essential part of modern transportation and essential infrastructure for economic development [1].

The flame and smoke will spread rapidly in the high-speed train carriage when a fire occurs. The safe evacuation of personnel is challenging, often causing heavy casualties and property losses [2]. The heat release rate (HRR) is the primary variable in high-speed train fire safety design and fire hazard evaluation. How to accurately calculate the HRR of high-speed train fire and analyze its influencing factors has become the focus of high-speed train fire research [2]. However, the existing calculation methods for the

fire HRR, such as the average heat release rate method [3] and Duggan method [4], can not reflect the influence of primary train components on the fire HRR, which makes the HRR calculated by the average heat release rate method and Duggan method much higher than the actual value.

The high-speed train fire is a complex combustion process. Its fire development process and HRR are mainly affected by the combustion characteristics of train materials, structures, and environmental factors [5]. The National Institute of Standards and Technology has conducted many combustion tests to analyze materials' flammability and smoke production characteristics [6]. They measured the HRR of seats by cone calorimeter [7] and studied the influence of seat combustion characteristics on fire spread. By comparing the small-scale test with the full-scale test, they found that the combustion characteristics of small-scale material can reflect the combustion characteristics of full-scale material in the actual combustion, consistent with the European Railway Research Institute [8].

With the extensive application of new composite materials in manufacturing train structures, the research on combustion tests of train material has not stopped. Kim *et al.* [9] used a small-scale material combustion test to study the fire-proof performance of train composite material. Lee *et al.* [10] conducted a combustion test to analyze the fire performance of train materials. Duggan [4] used a cone calorimeter to carry out many combustion tests of train materials. The research results showed that different radiation intensities should be used for different structure surfaces in the material combustion test. For example, the radiation intensity received by the ceiling, sidewall, and floor material surface should be 50, 35, and 25 kW/m<sup>2</sup>, respectively. This study provides a reference for selecting radiation intensity in the high-speed train material combustion test.

From 2000 to 2003, the Commonwealth Scientific and Industrial Research Organisation (CSIRO) conducted a series of full-scale train fire experiments. The results showed that the fire spread characteristics in the carriage are related to the layout of the train carriage [2]. The number of combustibles and the relative position of combustibles has a significant impact on the fire spread characteristics, which are the primary factors in controlling the flame spread [11]. Although scholars have researched the combustion characteristics of train materials and fire spread characteristics, there is little research on the combustion characteristics of train structures.

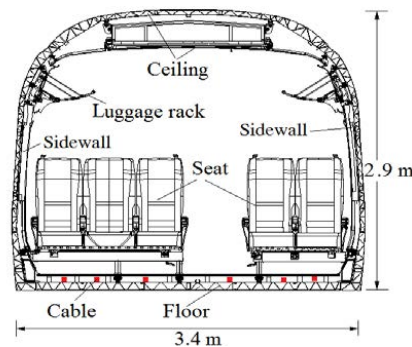
Taking a high-speed train in China as the research object, this paper studies the influence of the primary components of high-speed trains on the fire HRR through numerical methods. The study results can provide a reference for establishing a calculation method for high-speed train fire HRR.

## 2 Material and component combustion experiments

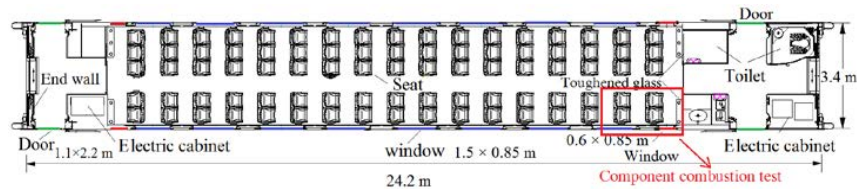
The heat release rate per unit area (HRRPUA) and the ignition temperature of materials are the main parameters of the high-speed train fire numerical simulation, which can be obtained by cone calorimeter [7] and ignition temperature tester [2] experiments, respectively. This section describes the high-speed train carriage's material and component combustion experiments in detail.

### 2.1 Material of train carriage

The structure of a high-speed train carriage is complex, and there are many interior decoration materials. The sidewalls, ceilings, luggage racks, seats, floors, and cables account for a large proportion and impact the fire spread characteristics in the carriage, which is the primary component of the high-speed train. Figure 1 shows the schematic diagram of the high-speed train carriage structure. The length is 24.2 m, the width is 3.4 m, and the height is 2.9 m.



(a) Train carriage sectional view



(b) Train carriage plan view

Figure 1: Schematics of the train structure.

The surface areas and thickness of the main combustible structures in the high-speed train carriage are given in Table 1. Figure 2 shows the proportion of the surface area of the main structure of the carriage.

Table 1: The surface area of each combustible structure of a train carriage.

| Structure    | Composition                 | Surface area (m <sup>2</sup> ) | Thickness (mm) | Radiation intensity (kW/m <sup>2</sup> ) |
|--------------|-----------------------------|--------------------------------|----------------|--|
| Ceiling      | Cold-resistant material     | 127.9                          | 20             | 50                                       |
|              | Interior ceiling material 1 | 63.8                           | 50             |  |
|              | Interior ceiling material 2 | 74.5                           | 50             |  |
|              | Interior ceiling material 3 | 5.5                            | 20             |  |
| Wall         | Cold-resistant material     | 92.6                           | 20             | 35                                       |
|              | Sidewall                    | 76.1                           | 30             |  |
|              | End wall                    | 15.3                           | 20             |  |
|              | Electrical cabinet wall     | 47.1                           | 20             |  |
|              | Toilet wall                 | 28.6                           | 20             |  |
|              | Window glass                | 22.4                           | 35             |  |
|              | Toughened glass             | 21.5                           | 20             |  |
| Floor        | Cold-resistant material     | 78.7                           | 25             | 25                                       |
|              | Floorcloth                  | 76.8                           | 15             |  |
|              | Floor                       | 78.7                           | 20             |  |
| Seat         | Seat armrest                | 73.0                           | 6              | 25                                       |
|              | Seat cushion                | 18.0                           | 50             |  |
|              | Seat back                   | 72.0                           | 50             |  |
| Cable        | Cable                       | 29.2                           | 6              | 50                                       |
| Luggage rack | Luggage rack                | 31.5                           | 20             | 50                                       |

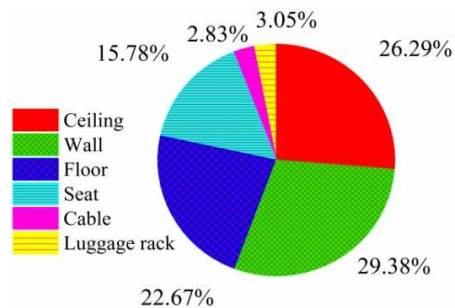


Figure 2: The proportion of the surface area of primary components of a train carriage.

Figure 1b also shows the component's location in the combustion experiment. This component includes two rows of seats and part of the end wall, sidewall, ceiling, luggage rack, and floor material. Figure 3 shows the actual view of the high-speed train component combustion experiment. During the experiment, propane fuel was used as an ignition source, the power of the ignition source was 15 kW, and the duration was 3 min.

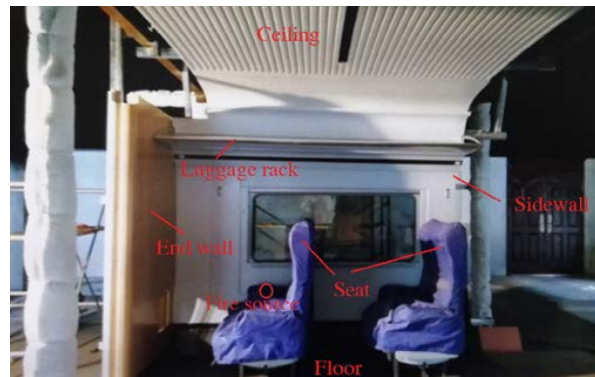


Figure 3: Actual view of the high-speed train component combustion test.

## 2.2 Experimental setup and method

Figure 4 presents a schematic of the cone calorimeter and ignition temperature tester. The radiation intensity received by the material surface of each component was determined according to the research results of Duggan [4].

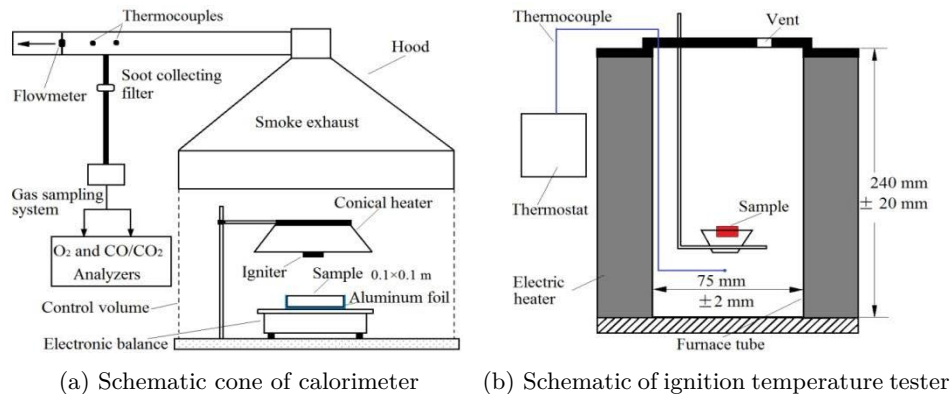


Figure 4: Schematics of the cone calorimeter and ignition temperature tester.

The cone calorimeter experiments in this study were performed following the ISO 5660-1 standard [12, 13]. Before the experiments, each material sample was placed in a constant-climate room at a temperature of  $23 \pm 2^\circ\text{C}$  and relative humidity of  $50 \pm 5\%$  for 48 h. Three combustion experiments were performed for each material to ensure the reproducibility of the experiment results, and the average of the three results was recorded.

The material ignition test was performed following the ASTM D1929 standard [2]. Before the experiment, each material sample was processed according to the method mentioned above. During the experiment, the sample was placed in the furnace tube. The temperature in the furnace tube was continuously adjusted using the thermostat. As the temperature in the furnace tube continued to rise to the point at which the material sample was just ignited, the temperature in the furnace tube was taken to be the ignition temperature of the material. The ignition temperature of each material was measured three times, and then the average value of the test data was taken.

### 2.3 Material heat release rate and ignition temperature

Figure 5 presents the HRRPUA of each combustible material of primary components in a high-speed train carriage. When analyzing the influence of the train's primary components on the fire HRR, replacing the material in the original carriage with different materials is necessary. The HRRPUA of each replacement material is shown in Fig. 6. The ignition temperatures of the combustible materials constituting the primary components of the high-speed train carriage are presented in Table 2.

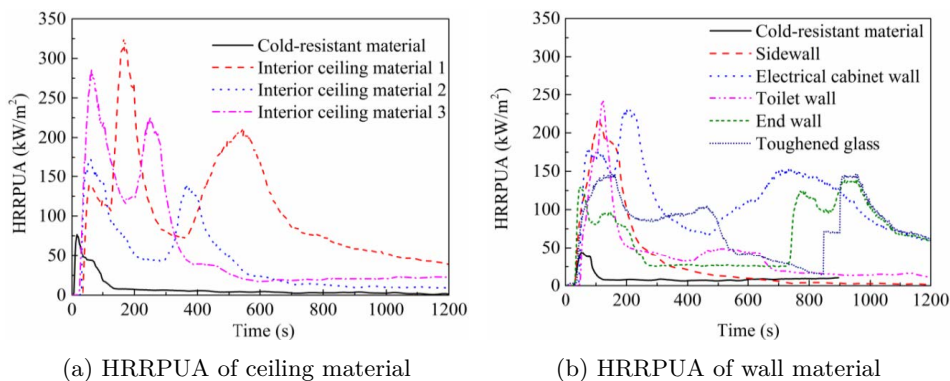
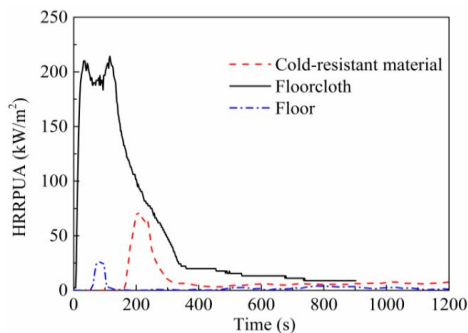
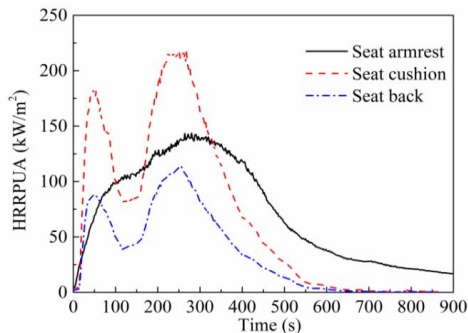


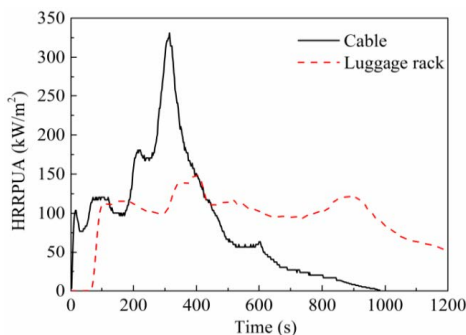
Figure 5: For caption see next page.



(c) HRRPUA of floor material

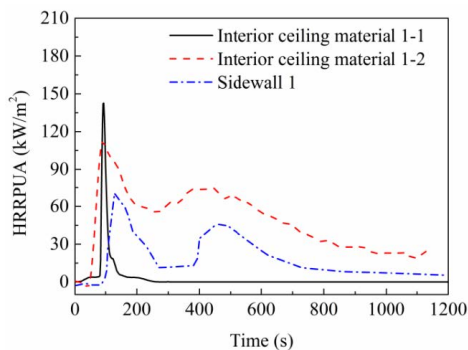


(d) HRRPUA of seat material

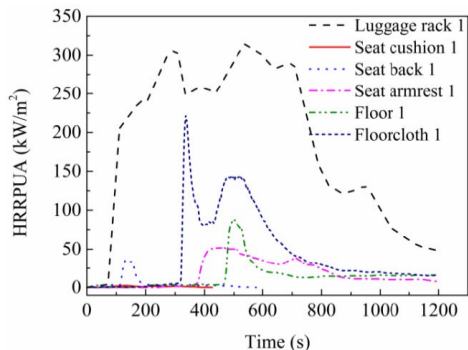


(e) HRRPUA of cable and luggage rack

Figure 5: The heat release rate per unit area of different combustible materials in the train carriage.



(a) Ceiling and wall



(b) Luggage rack, seat, and floor

Figure 6: The heat release rate per unit area of each replaced material.

Table 2: Ignition temperatures of combustible materials in high-speed trains.

| Structure    | Composition                 | Ignition temperature (°C) |
|--------------|-----------------------------|---------------------------|
| Ceiling      | Cold-resistant material     | 278                       |
|              | Interior ceiling material 1 | 450                       |
|              | Interior ceiling material 2 | 520                       |
|              | Interior ceiling material 3 | 526                       |
| Wall         | Cold-resistant material     | 536                       |
|              | Sidewall                    | 520                       |
|              | End wall                    | 440                       |
|              | Electrical cabinet wall     | 480                       |
|              | Toilet wall                 | 470                       |
|              | Window glass                | 600                       |
|              | Toughened glass             | 530                       |
| Floor        | Cold-resistant material     | 450                       |
|              | Floorcloth                  | 780                       |
|              | Floor                       | 433                       |
| Seat         | Seat armrest                | 350                       |
|              | Seat cushion                | 460                       |
|              | Seat back                   | 460                       |
| Cable        | Cable                       | 350                       |
| Luggage rack | Luggage rack                | 526                       |

### 3 Numerical method

#### 3.1 Governing equations

During a fire, the flow of smoke is a three-dimensional, unsteady, and compressible turbulent flow. The Fire Dynamics Simulator (FDS, version 6.7.4) [14–17] program is used to simulate the train fire (a computational fluid dynamics (CFD) model of fire-driven fluid flow), and the turbulent flow of smoke is solved by the large eddy simulation (LES) [18–20]. The governing equations are shown below [21–24]:

Mass conservation equation

$$\frac{\partial \rho}{\partial t} + \nabla \cdot U \rho = 0, \quad (1)$$

where  $t$  is the time,  $\rho$  and  $U$  are the density and velocity of airflow, respectively.

Component conservation equation

$$\frac{\partial(\rho Y_i)}{\partial t} + \nabla \cdot \rho Y_i U = \nabla \cdot \rho D_i \nabla Y_i + \dot{m}_i''', \quad (2)$$

where  $\dot{m}_i'''$  is the mass formation rate of the  $i$ th component in unit volume,  $D_i$  is the component mass diffusion coefficient, and  $Y_i$  is the volume fraction of the  $i$ th component.

Momentum conservation equation

$$\frac{\partial(\rho U)}{\partial t} + \nabla \cdot \rho U U + \nabla P = \rho g + f + \nabla \cdot \tau_{ij}, \quad (3)$$

$$\tau_{ij} = \mu \left[ 2S_{ij} - \frac{2}{3} \delta_{ij} (\nabla \cdot U) \right], \quad (4)$$

$$S_{ij} = \frac{1}{2} \left( \frac{\partial u_i}{\partial x_j} + \frac{\partial u_j}{\partial x_i} \right), \quad (5)$$

$$\delta_{ij} = \begin{cases} 1, & i = j, \\ 0, & i \neq j, \end{cases} \quad (6)$$

where  $g$  is the gravitational acceleration,  $f$  is the force (except gravity),  $\tau_{ij}$  is the viscous stress tensor,  $S_{ij}$  is the strain tensor, and  $\mu$  is the kinematic viscosity.

Energy conservation equation

$$\frac{\partial(\rho h_s)}{\partial t} + \nabla \cdot U \rho h_s = \frac{Dp}{Dt} - \nabla \cdot \mathbf{q}_r + \nabla \cdot U P + \nabla \cdot k \nabla T + \sum_i \nabla \cdot h_{s,i} \rho D_i \nabla Y_i, \quad (7)$$

where  $h_s$  is the sensible enthalpy,  $\mathbf{q}_r$  is the radiant heat flux vector,  $k$  is the coefficient of heat conductivity, and  $T$  is the thermodynamic temperature.

Meanwhile, the state equation of ideal gas was also needed. Its form is shown below:

$$P = \rho R_g T, \quad (8)$$

where  $P$  is the pressure, and  $R_g$  is the specific gas constant.

When LES is used to solve turbulent flow, the governing equations need to be transformed:

$$\frac{\partial \bar{u}_i}{\partial t} + \frac{\partial \bar{u}_i \bar{u}_j}{\partial x_j} = -\frac{1}{\rho} \frac{\partial \bar{P}}{\partial x_i} + \mu \frac{\partial^2 \bar{S}_{ij}}{\partial x_j \partial x_j} - \frac{\partial(\tau_{ij})}{\partial x_j}, \quad (9)$$

$$\bar{S}_{ij} = \frac{1}{2} \left( \frac{\partial \bar{u}_i}{\partial x_j} + \frac{\partial \bar{u}_j}{\partial x_i} \right), \quad (10)$$

where the overbar indicates filtering,  $\tau_{ij}$  represents the effect of small eddy on large eddy, and it needs to be calculated by establishing a subgrid scale model, such as the Smagorinsky model:

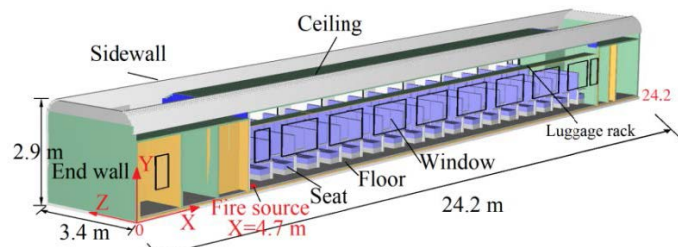
$$\tau_{ij} - \frac{1}{3}\tau_{kk} \cdot \delta_{ij} = -2\bar{S}_{ij} \cdot \mu_{LES}, \quad (11)$$

$$\mu_{LES} = \rho (C_s \Delta)^2 \left[ 2\bar{S}_{ij} \cdot \bar{S}_{ij} - \frac{2}{3}(\nabla \cdot \bar{u})^2 \right]^{\frac{1}{2}}, \quad (12)$$

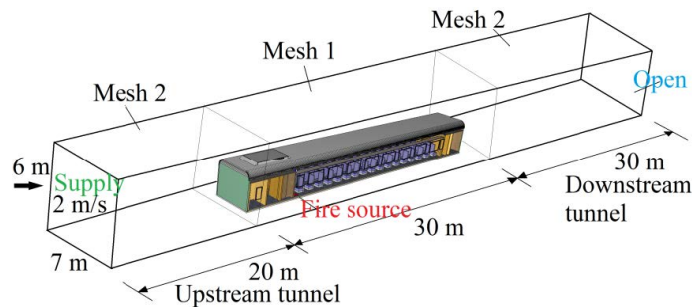
where  $\mu_{LES}$  is the turbulent viscosity coefficient at a subgrid scale,  $C_s$  is the Smagorinsky constant,  $u_i$ ,  $u_j$  are the velocity components in  $x$  and  $y$  direction, and  $x_i$ ,  $x_j$  represent the Cartesian coordinates.

### 3.2 Numerical model

Figure 7a shows the numerical model of the high-speed train fire based on the high-speed train carriage structure. The HRRPUA method is used



(a) Numerical model of a train fire



(b) Computational domain of the numerical model

Figure 7: Numerical model of a train fire and the computational domain of the model.

for fire simulation [25, 26]. In this method, it is necessary to input the curve of the HRRPUA and the ignition temperature of each structural material (as shown in Section 2.3). Figure 7b shows the computational domain of the numerical model for a high-speed train fire in a railway tunnel. The width of the tunnel is 7 m, and the height is 6 m. The length of the upstream tunnel is 20 m, and the length of the downstream tunnel is 30 m. The ‘supply’ boundary condition is applied to the tunnel entrance, and the velocity is 2 m/s [2]. The ‘open’ boundary condition is applied to the tunnel exit, and the ‘inert’ boundary condition is applied to the tunnel wall surface.

In this study, the window rupture temperature is 600°C [27]. The door on one side of the train carriage is open before the fire simulation. The fire source is at the end wall corner of the carriage (as shown in Fig. 7a). The fire source power is 150 kW, and the duration is 8 min [2].

### 3.3 Numerical mesh

As shown in Fig. 7b, the computational domain is divided into three regions. The mesh around and inside the train carriage is designated as ‘Mesh 1’, and that in the upstream tunnel and downstream tunnel is designated as ‘Mesh 2’. The size of Mesh 1 is between 0.06 m and 0.10 m; Mesh 2 is twice as large. Figure 8 presents the HRR of train fires (original carriage)

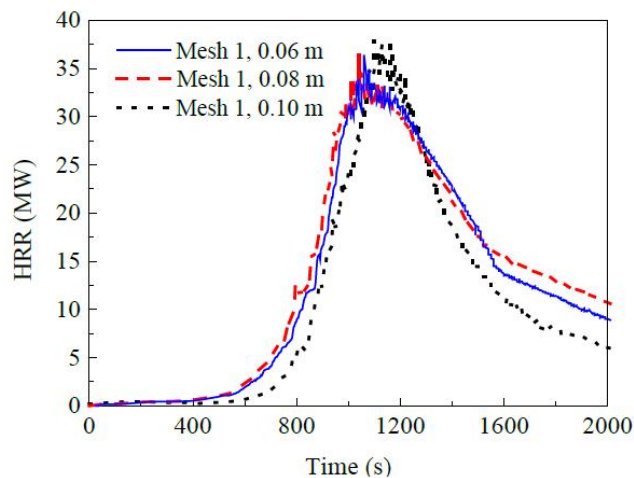


Figure 8: HRR of the train fire with different mesh sizes.

with different mesh sizes. As shown in Figure 8, when the size of Mesh 1 is reduced from 0.08 m to 0.06 m, the difference in the HRR curve of the train carriage fire is minimal. Therefore, in this study, the size of Mesh 1 is set as 0.08 m, the size of Mesh 2 is set as 0.16 m, and the total number of meshes is 2.95 million.

### 3.4 Comparison with component combustion experiment

Figure 9a shows the FDS model established according to the component structure. The fire source is set on the seat surface. The fire source power is 15 kW, and the duration is 3 min. The mesh size of the FDS model is 0.08 m. Figure 9b presents a comparison between the HRRs of the numerical simulation and the component combustion experiment. The numerical simulation is consistent with the experimental conditions, indicating that the numerical method employed in this study can accurately simulate high-speed train fires.

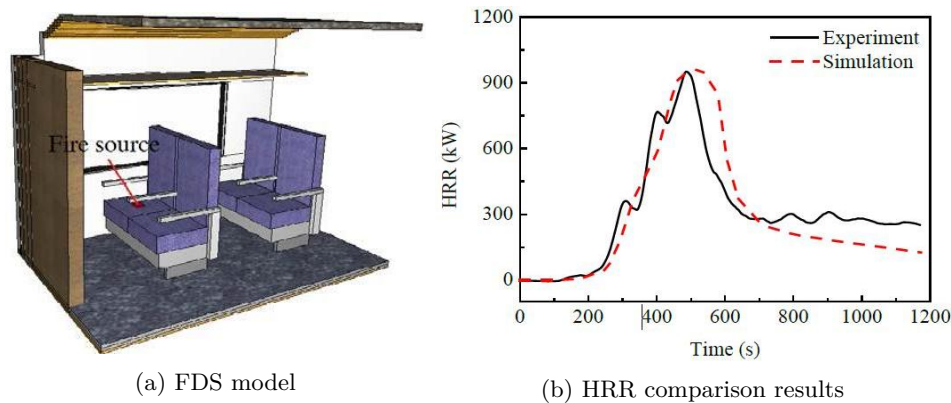


Figure 9: The Fire Dynamics Simulator model and heat release rate comparison results.

## 4 Results and discussion

In this section, the influence of ceilings, sidewalls, luggage racks, seats, and floors on the HRR of high-speed train fire is studied. The fire cases are shown in Table 3. The peak HRRPUA of different materials with the same structure is also given in Table 3.

Table 3: Case for fire simulation.

| Case | Original material   |                                     | Replaced material   |                                     |
|------|---|-------------------------------------|---|-------------------------------------|
|      | Material  | Peak HRRPUA<br>(kW/m <sup>2</sup> ) | Material  | Peak HRRPUA<br>(kW/m <sup>2</sup> ) |
| A    | The HRRPUA for all materials was shown in Fig. 5 (original carriage). |                                     |   |                                     |
| B    | Ceiling: interior ceiling material 1                                  | 326                                 | Ceiling: interior ceiling material 1-1                            | 140                                 |
| C    | Ceiling: interior ceiling material 1                                  | 326                                 | Ceiling: interior ceiling material 1-2                            | 110                                 |
| D    | Wall: sidewall  | 219                                 | Wall: sidewall 1  | 123                                 |
| E    | Luggage rack  | 150                                 | Luggage rack 1  | 319                                 |
| F    | Luggage rack  | 150                                 | Luggage rack 2: non-combustible                                   | 0                                   |
| G    | Seat: seat armrest<br>Seat: seat cushion<br>Seat: seat back           | 144<br>218<br>114                   | Seat: seat armrest 1<br>Seat: seat cushion 1<br>Seat: seat back 1 | 52<br>2.5<br>36                     |
| H    | Floor: floor cloth<br>Floor: floor                                    | 221<br>26                           | Floor: floor cloth 1<br>Floor: floor 1                            | 223<br>88                           |

#### 4.1 Effects of ceilings

The interior ceiling material 1 is the primary material of the ceilings, located on the inner surface of the carriage. Previous papers [1, 2] have studied the fire spread characteristics in the train carriage. The results indicated that when the fire occurs in the carriage, the flame spreads along with the ceiling to both ends of the carriage, causing the materials at both ends of the carriage to burn. The seat and floor then burn owing to the heat radiation from the ceiling. Therefore, whether the fire can spread in the carriage mainly depends on the combustion characteristics of the ceiling materials.

Figure 10 shows the HRR of train carriage fire under different interior ceiling materials 1. The peak HRRPUA of the material under the different cases is shown in Table 3. It can be seen from Fig. 10 that the peak HRR of Case A is 36.4 MW. However, the peak HRRs of Case B and Case C are 19.4 MW and 16.5 MW, respectively. Compared with Case A, the peak HRR of Case B and Case C decreased by 46.7% and 54.7%, respectively. Therefore, the peak HRR of train carriage fire decreases with the decrease of peak HRRPUA of interior ceiling material 1.

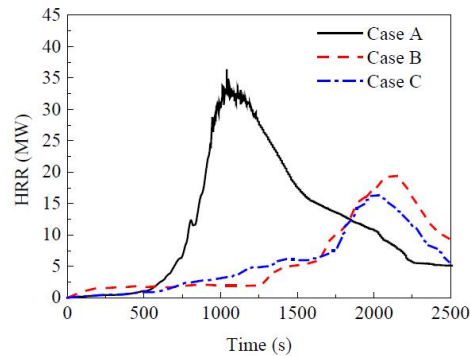


Figure 10: HRR under different ceiling materials.

The time when the train fire reaches the peak HRR is an important parameter in the design fire for train carriages [19]. It can be found from Fig. 10 that the interior ceiling material 1 has a significant influence on the time to peak HRR. The time to peak HRR of the train carriage fire in Case A is approximately 1040 s, while that in Case B and Case C is 2140 s and 2018 s, respectively. Therefore, the interior ceiling material with low HRRPUA can delay the time to peak HRR of the train carriage fire.

Figure 11 shows the HRR growth rate of train carriage fire with different interior ceiling materials 1. The HRR growth rate is calculated as follows:

$$\frac{dQ}{dt} = \frac{\Delta Q}{\Delta t}, \quad (13)$$

where  $Q$  represents the HRR of the fire,  $t$  represents time,  $dQ/dt$  represents the HRR growth rate of the fire, and  $\Delta t = 60$  s. As shown in Fig. 11, the

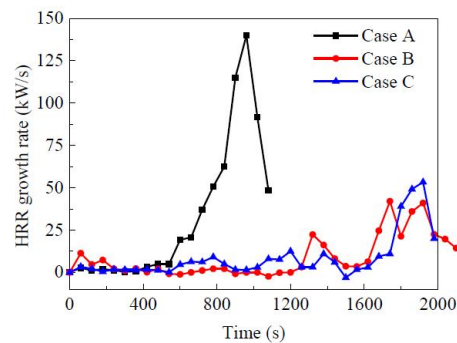


Figure 11: Increasing rate of the train fire HRR under different ceiling materials.

maximum HRR growth rate of Case A is 140 kW/s, while that of Case B and Case C is 41 kW/s and 53 kW/s, respectively. Before 580 s, the HRR growth rate of carriage fire under three cases is relatively close, but after 580 s, the fire HRR of Case A increases rapidly. However, the HRR growth rate of Case B and Case C is low in the whole fire development process.

Figure 12 shows the fire spreading process in the train carriage under three cases. For Case A, when the fire HRR reached the peak, the whole carriage was burning. For Case B and Case C, when the fire HRR reached the peak, the combustion intensity in the train carriage was weak, and some seat and floor materials were not burned. The reason for this phenomenon is that the peak HRRPUA of interior ceiling material 1 in Case B and Case C was low, which reduces the combustion intensity of ceiling material, resulting in the heat radiation on the surface of the seat and floor material being reduced, and some materials were not ignited.

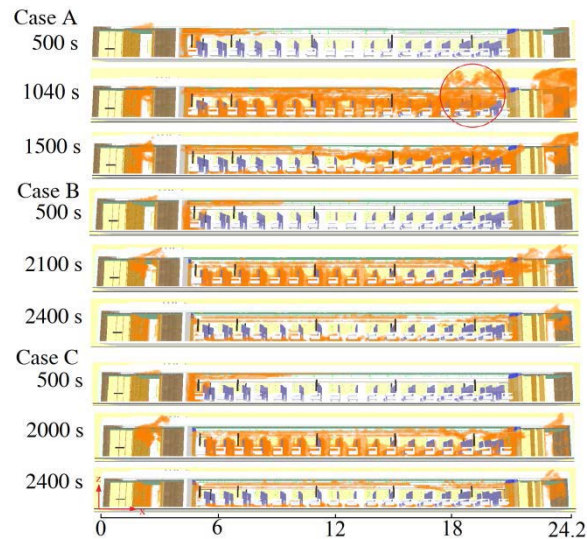


Figure 12: Fire spread in the train carriage.

Figure 13 shows the smoke temperature distribution at 0.1 m below the carriage ceiling in Case A and Case C, respectively. The measuring points are arranged along the train carriage centre line, and the coordinate origin is located at the end wall (as shown in Fig. 7a). It can be seen from Fig. 13 that before the fire HRR reaches the peak, the temperature near the fire source ( $x = 4.7$  m) is the highest, and the temperature at both ends of the train carriage is lower. After the fire HRR reaches the peak, the temperature

at the end of the carriage on the right side of the fire source increases. The main reason for this phenomenon is the fire flashover characteristics in the carriage. The previous paper [1] studied the characteristics of fire flashover in train carriages. The results showed that when the HRR reaches the peak, the flashover intensity of the carriage end door area far away from the fire source (as shown in Fig. 12) is the largest, which makes the temperature of the end door area of the carriage increase.

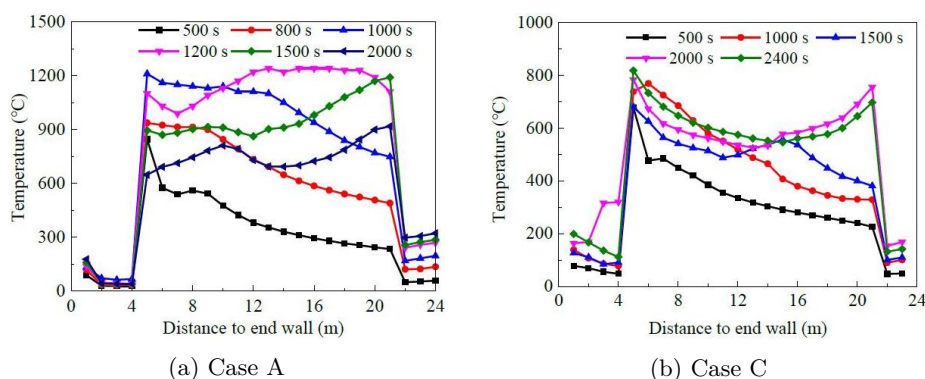


Figure 13: Distribution of smoke temperature below the ceiling at various times.

## 4.2 Effects of sidewalls

This section analyzes the influence of sidewall materials on the HRR of train carriage fire. Figure 14 shows the HRR of train carriage fire under two

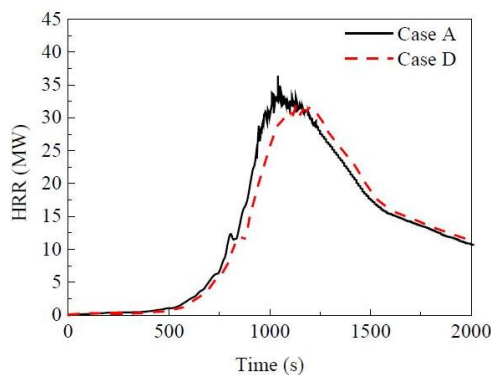


Figure 14: HRR under different sidewall materials.

cases. The peak HRRs for Case A and Case D are 36.4 MW and 31.5 MW, respectively. Compared with Case A, the decreased ratio of peak HRR of Case D is 13.5%. Moreover, the time to peak HRR in Case D is 1140 s, which is 100 s later than in Case A.

Figure 15 shows the temperature distribution on the surface of the sidewall. The temperature measuring point is 1.2 m away from the floor. The maximum temperature of the sidewall surface in Case A and Case D is 1100°C and 980°C, respectively, and the temperature difference is minimal. From the simulation results of the peak HRR and the time to peak HRR in Case A and Case D, it can be seen that reducing the HRRPUA of the sidewall material can not significantly reduce the HRR of the train carriage fire and delay the time to peak HRR. However, there are two reasons for this phenomenon: the first one is that the surface area of sidewall materials is 76.1 m<sup>2</sup>, which accounts for 7.4% of the total area of train materials. The heat generated by the combustion of sidewall materials accounts for a small proportion of the heat generated by whole train combustion, so it has little impact on the peak HRR of the carriage fire; another reason is that the temperature difference of sidewall surface under different sidewall materials is small, which will not have a significant impact on the combustion of the seat and floor materials.

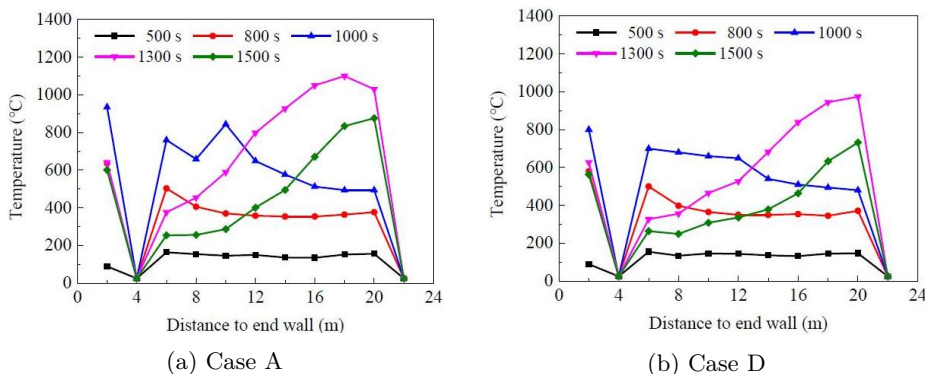


Figure 15: Temperature distribution on the sidewall surface in the carriage.

### 4.3 Effects of luggage racks

Figure 16 shows the HRR of the train carriage fire with different luggage rack materials. The peak HRRs in Case A, Case E, and Case F are 36.4, 36.7, and 34.1 MW, respectively. The peak HRR increases with the increase

of luggage rack material's HRRPUA, but the difference is small. In the three cases, the time to peak HRR is 1040, 1060, and 1240 s, respectively. From the comparison results of the peak HRR of the train carriage fire, whether the luggage rack is combustible or not, the impact of the luggage rack on the peak HRR of the train carriage fire is small. The main reason is that the area of the luggage rack accounts for a small proportion (3.05%) of the train carriage area.

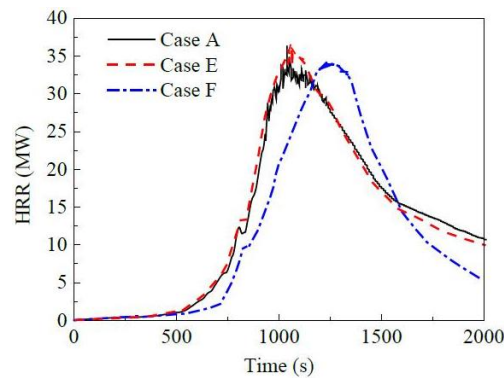


Figure 16: HRR under different luggage rack materials.

As shown in Fig. 16, when the carriage is equipped with a combustible luggage rack, the difference in the time to peak HRR of the train carriage fire is minimal. However, when the non-combustible luggage rack is used, the maximum delay time of the carriage fire HRR to the peak is 200 s. Figure 17 shows the flame spread in the initial growth stage of the fire in the train carriage. When a combustible luggage rack is used, the flame can spread to the ceiling, while when using a non-combustible luggage rack, the flame can not spread to the ceiling in the initial growth stage of fire.

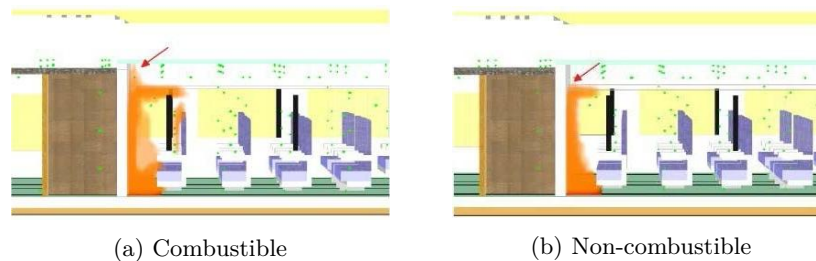


Figure 17: Influence of luggage rack on flame spread.

#### 4.4 Effects of seats

Figure 18 shows the HRR of the train carriage fire in Case A and Case G. The peak HRR of Case A is 36.4 MW, and that of Case G is 20.1 MW. Compared with Case A, the reduction ratio of peak HRR of Case G is 44.8%. In Case G, the time to peak HRR is 1480 s, which is 440 s later than in Case A. Therefore, the seat material with low HRRPUA can significantly reduce the peak HRR of the train carriage fire and delay the time to peak HRR.

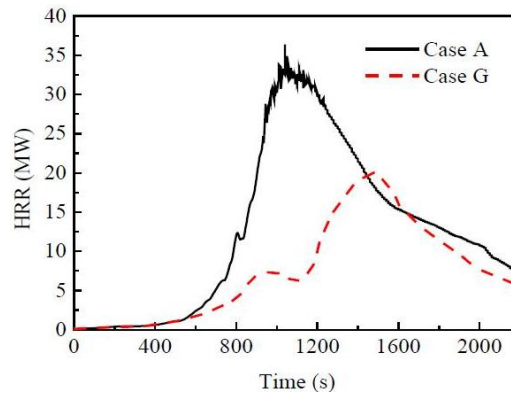


Figure 18: HRR under different seat materials.

Figure 19 shows the HRR growth rate of the carriage fire in Case A and Case G. The maximum HRR growth rate is 140 kW/s and 73 kW/s, respectively. For Case G, the fire HRR growth rate decreases significantly when

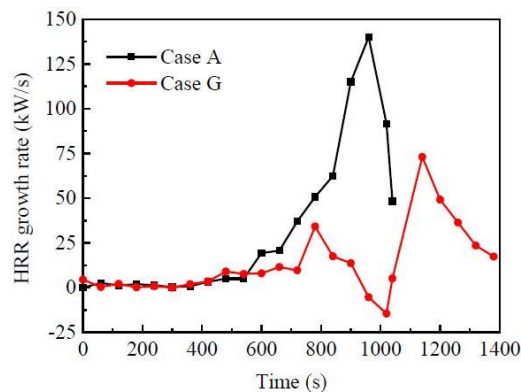


Figure 19: Increasing rate of the train fire HRR under different seat materials.

the fire develops from 780 s to 1020 s. After 1020 s, the fire HRR increases rapidly. The reason for this phenomenon is that: in the initial growth stage of fire development, combustion mainly occurs on the ceiling and the seat surface near the fire source. However, the HRRPUAs of seat materials are low, and the amount of heat generated by combustion is low. With the mass consumption of ceiling material, the HRR of the whole carriage is decreased. Then under the heat radiation of the ceiling, the rest of the seat and floor materials are ignited, and the fire HRR increases rapidly.

#### 4.5 Effects of floors

Figure 20 shows the comparison results of fire HRR of Case A and Case H. As shown in Fig. 20, the peak HRR of Case H is 36.9 MW, which is 0.5 MW larger than in Case A. Moreover, the difference in time to peak HRR between the two cases is minimal, and the time to peak HRR is approximately 1040 s.

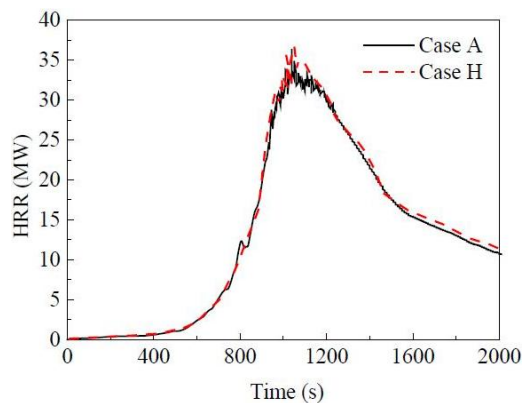


Figure 20: HRR under different floor materials.

Figure 21 shows the temperature distribution in the train carriage of Case A. The temperature near the fire source is the highest in the initial growth stage of the fire development in the carriage. With the development of the fire, the temperature in the carriage increases, and the high-temperature area gradually spreads to the right carriage of the fire source. At 1040 s, the high-temperature area spreads to the whole carriage, and the temperature of the whole ceiling material surface is about 1000°C. At this time, the fire heat release rate reaches a peak.

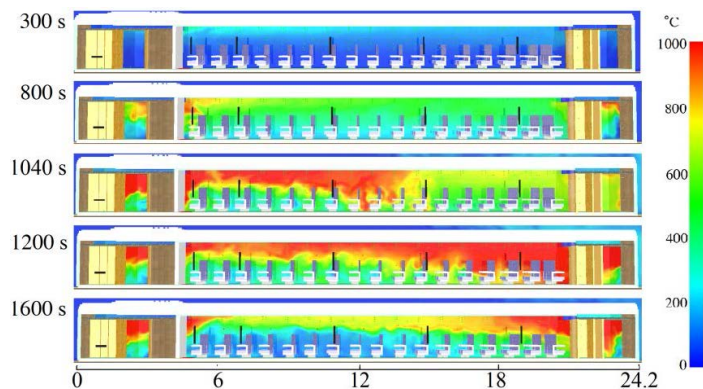


Figure 21: Temperature distribution in the train carriage.

Figure 22 shows the temperature distribution of the floor surface along the length of the train carriage. At the same computing time, the difference in temperature between Case A and Case H is very small. When the HRR of the train carriage fire reaches the peak (at 1040 s), the maximum temperature of the floor surface is approximately  $740^{\circ}\text{C}$ , and the temperature at both ends of the carriage is higher than that in the middle (approximately  $360\text{--}480^{\circ}\text{C}$ ). However, as shown in Table 2, the ignition temperatures of floor cold-resistant, floor cloth, and floor materials are  $450$ ,  $780$ , and  $433^{\circ}\text{C}$ , respectively. Therefore, only a tiny amount of floor material is ignited before the carriage fire reaches its peak. In the late stage of fire development, the temperature of the floor surface at the end of the carriage increases,

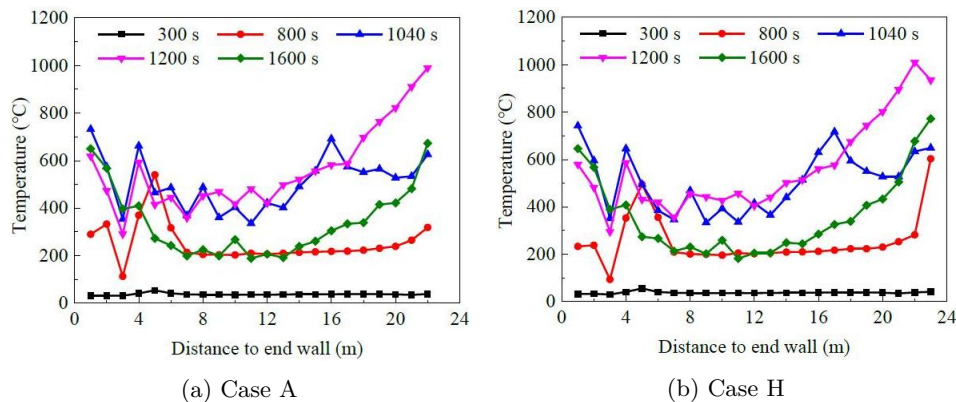


Figure 22: Temperature distribution on the floor surface in the carriage.

and the combustion intensity of the floor material at the end of the carriage increases.

## 5 Conclusions

In this study, based on the HRRPUA and ignition temperature of the high-speed train materials, a numerical model of the high-speed train fire is established. The accuracy of the numerical method is verified by comparing it with the component combustion experiments. Then, the effects of the ceilings, sidewalls, luggage racks, seats, and floors on carriage fire HRR are studied. The following conclusions are drawn:

- The HRRPUA of ceiling material dramatically influences the peak HRR and the time to peak HRR of high-speed train carriage fire. When the peak HRRPUA of interior ceiling material decreases from  $326 \text{ kW/m}^2$  to  $110 \text{ kW/m}^2$ , the peak HRR of the train carriage fire decreases from 36.4 MW to 16.5 MW, with a reduction ratio of 54.7%. The time to peak HRR increased from 1040 s to 2018 s.
- The sidewall material has a certain influence on the HRR of high-speed train carriage fire. When the peak HRRPUA of sidewall material decreases from  $219 \text{ kW/m}^2$  to  $123 \text{ kW/m}^2$ , the peak HRR decreases from 36.4 MW to 31.5 MW, with a reduction ratio of 13.5%. Moreover, the influence of sidewall material on the surface temperature of the sidewall is small.
- The combustible luggage rack has little effect on the HRR of high-speed train carriage fire. However, the non-combustible luggage rack can delay the time when the HRR reaches its peak.
- The HRRPUA of seat material greatly influences the HRR of high-speed train carriage fire. When seat materials with low HRRPUA are used, the peak HRR of carriage fire is 20.1 MW, and the reduction ratio is 44.8%. Moreover, the time to peak HRR is delayed by 440 s.
- The combustion intensity of the floor materials in the high-speed train carriage is low. The HRRPUA of the floor materials has little effect on the HRR of the high-speed train carriage fire.

Although the research in this paper was carried out for specific train types, the research conclusions were also applicable to other high-speed train fires.

Moreover, the research results can provide guidance for the design of the high-speed train structure and fire protection, as well as the establishment of the calculation method of the high-speed train fire HRR.

*Received 10 January 2023*

## References

- [1] Bi H.Q., Zhou Y.L., Wang H.L., Gou Q.L., Liu X.X.: *Characteristics of fire in high-speed train carriages*. J. Fire Sci. **38**(2020), 1, 75–95. doi: [10.1177/0734904119894527](https://doi.org/10.1177/0734904119894527)
- [2] Zhou Y.L., Wang H.L., Bi H.Q., Liu X.X., Gou Q.L.: *Heat release rate of high-speed train fire in railway tunnels*. Tunn. Undergr. Sp. Tech. **105**(2020), 103563. doi: [10.1016/j.tust.2020.103563](https://doi.org/10.1016/j.tust.2020.103563)
- [3] White N.: *Fire development in passenger trains*. PhD thesis, Victoria University, Melbourne 2010.
- [4] Duggan G.J.: *Fire hazards, testing, materials and products*. In Proc. Conf. on Usage of ISO 5660 Data in UK Railway Standards and Fire Safety Cases, Rubber and Plastics Institute (Rapra), Shrewsbury, 13 March 1997, 1–8.
- [5] Craig M., Asim T.: *Numerical investigations on the propagation of fire in a railway carriage*. Energies **13**(2020), 19, 4999. doi: [10.3390/en13194999](https://doi.org/10.3390/en13194999)
- [6] Peacock R.D., Braun E.: *Fire Tests of Amtrak Passenger Rail Vehicle Interiors. Final Report*. 1978–1983 (Natl. Bur. Stand. Tech. Note 1193). NIST TN 1193, Washington, DC, 1984. doi: [10.6028/Nbs.tn.1193](https://doi.org/10.6028/Nbs.tn.1193)
- [7] Lslam M.T., Klinger J.L., Reza M.T.: *Evaluating combustion characteristics and combustion kinetics of corn stover-derived hydrochars by cone calorimeter*. Chem. Eng. J. **452**(2023), 2, 139419. doi: [10.1016/j.cej.2022.139419](https://doi.org/10.1016/j.cej.2022.139419)
- [8] Hirschler M.M.: *Use of heat release rate to predict whether individual furnishings would cause self propagating fires*. Fire Safety J. **32**(1999), 3, 273–296. doi: [10.1016/S0379-7112\(98\)00037-X](https://doi.org/10.1016/S0379-7112(98)00037-X)
- [9] Kim J.S., Jeong J.C., Cho S.H., Seo S.I.: *Fire resistance evaluation of a train car body made of composite material by large scale tests*. Compos. Struct. **83**(2008), 3, 295–303. doi: [10.1016/j.compstruct.2007.04.022](https://doi.org/10.1016/j.compstruct.2007.04.022)
- [10] Lee D.H., Park W.H., Jung W.S., Hwang J.H.: *Fire test of old type interiors of subway vehicle in ISO 9705 room*. J. Korean Soc. Rail. **13**(2010), 5, 481–487.
- [11] Lönnermark A., Ingason H., Li Y.Z., Kumm M.: *Fire development in a 1/3 train carriage mock-up*. Fire Safety J. **91**(2017), 432–440. doi: [10.1016/j.firesaf.2017.03.016](https://doi.org/10.1016/j.firesaf.2017.03.016)
- [12] Ryu S., Mun S.Y., Hwang C.H.: *Effect of the cone heater scale compliant with the ISO 5660 standard on spatial uniformity of radiant heat flux*. Fire Sci. Eng. **34**(2020), 5, 27–33. doi: [10.7731/KIFSE.ad1befcd](https://doi.org/10.7731/KIFSE.ad1befcd)
- [13] Knez N., Kariž M., Knez F., Ayrilmis N., Kuzman M.K.: *Effects of selected printing parameters on the fire properties of 3d-printed neat polylactic acid (PLA) and wood/PLA composites*. J. Renew. Mater. **9**(2021), 11, 1883–1895. doi: [10.32604/jrm.2021.016128](https://doi.org/10.32604/jrm.2021.016128)

- [14] Wang Z.Y., Ji J., Tan T.T., Gao Z.H., Zhou Y., Zhou F.: *Numerical study on the critical criterion for predicting the plug-holing under lateral mechanical exhaust in tunnel fires: Considering the effect of smoke flow in longitudinal direction*. Tunn. Undergr. Sp. Tech. **128**(2022), 104666. doi: [10.1016/j.tust.2022.104666](https://doi.org/10.1016/j.tust.2022.104666)
- [15] Fan, C., Zhang, L., Jiao, S., Yang, Z., Li, M., Liu, X.: *Smoke spread characteristics inside a tunnel with natural ventilation under a strong environmental wind*. Tunn. Undergr. Sp. Tech. **82**(2018), 99–110. doi: [10.1016/j.tust.2018.08.004](https://doi.org/10.1016/j.tust.2018.08.004)
- [16] Liu Y., Shen J., Ma J., Li G., Zhao Z., Ni X., Wang X.: *Laser-based measurement and numerical simulation of methane-air jet flame suppression with water mist*. Process Saf. Environ. Protect. **148**(2021), 1033–1047. doi: [10.1016/j.psep.2021.02.028](https://doi.org/10.1016/j.psep.2021.02.028)
- [17] Zhao J., Xu Z., Ying H., Guan X., Chu K., Tagne S.M.S., Tao H.: *Study on smoke spread characteristic in urban interval tunnel fire*. Case Stud. Therm. Eng. **30**(2022), 101755. doi: [10.1016/j.csite.2022.101755](https://doi.org/10.1016/j.csite.2022.101755)
- [18] Zhang M., Ong J.C., Pang K.M., Bai X.S., Walther J.H.: *Large eddy simulation of soot formation and oxidation for different ambient temperatures and oxygen levels*. Appl. Energ., **306**(2022), 118094. doi: [10.1016/j.apenergy.2021.118094](https://doi.org/10.1016/j.apenergy.2021.118094)
- [19] Liu Y.X., Liu C.H., Brasseur G.P., Chao C.Y.H.: *Proper orthogonal decomposition of large-eddy simulation data over real urban morphology*. Sustain. Cities Soc. **25**(2022), 104324. doi: [10.1016/j.scs.2022.104324](https://doi.org/10.1016/j.scs.2022.104324)
- [20] Peterson D.M.: *Simulation of a round supersonic combustor using wall-modelled large eddy simulation and partially-stirred reactor models*. P. Combust. Inst. (2022). doi: [10.1016/j.proci.2022.08.120](https://doi.org/10.1016/j.proci.2022.08.120)
- [21] Zhou Y.L., Wang H.L., Bi H.Q., Wang J.: *Experimental and numerical study of aerodynamic pressures on platform screen doors at the overtaking station of a high-speed subway*. Build. Environ. **191**(2021), 107582. doi: [10.1016/j.buildenv.2020.107582](https://doi.org/10.1016/j.buildenv.2020.107582)
- [22] Bi H.Q., Wang Z.H., Wang H.L., Zhou Y.L.: *Aerodynamic phenomena and drag of a maglev train running dynamically in a vacuum tube*. Phys. Fluids **34**(2022), 9, 096111. doi: [10.1063/5.0104819](https://doi.org/10.1063/5.0104819)
- [23] Korib K., Ihaddadene N., Bouakkaz R., Khelili Y.: *Numerical simulation of forced convection of nanofluid around a circular cylinder*. Arch. Thermodyn. **40**(2019), 2, 3–16. doi: [10.24425/ather.2019.129539](https://doi.org/10.24425/ather.2019.129539)
- [24] Saeed F.R., Al-Dulaimi M.A.: *Numerical investigation for convective heat transfer of nanofluid laminar flow inside a circular pipe by applying various models*. Arch. Thermodyn. **42**(2021), 1, 71–95. doi: [10.24425/ather.2021.136948](https://doi.org/10.24425/ather.2021.136948)
- [25] Beji T., Merci B.: *Numerical simulations of a full-scale cable tray fire using small-scale test data*. Fire Mater. **43**(2019), 5, 486–496. doi: [10.1002/fam.2687](https://doi.org/10.1002/fam.2687)
- [26] Chen Y.J., Shu C.M., Ho S.P., Kung H.C., Chien S.W., Ho H.H., Hsu W.S.: *Analysis of smoke movement in the Hsuehshan tunnel fire*. Tunn. Undergr. Sp. Tech. **84**(2019), 142–150. doi: [10.1016/j.tust.2018.11.007](https://doi.org/10.1016/j.tust.2018.11.007)
- [27] Li Y.Z., Ingason H.: *A new methodology of design fires for train carriages based on exponential curve method*. Fire Technol. **52**(2016), 5, 1449–1464. doi: [10.1007/s10694-015-0464-3](https://doi.org/10.1007/s10694-015-0464-3)